Linking mantle plumes, large igneous provinces and environmental catastrophes

Article *in* Nature · September 2011

DOI: 10.1038/nature10385 · Source: PubMed

8 authors, including:

Stephan V. Sobolev
Helmholtz-Zentrum Potsdam - Deutsches Ge…
192 PUBLICATIONS **5,666** CITATIONS
SEE PROFILE

Alexander V Sobolev
Université Grenoble Alpes
235 PUBLICATIONS **7,463** CITATIONS
SEE PROFILE

Nadezhda Alexandrovna Krivolutskaya, N. A. …
Russian Academy of Sciences
68 PUBLICATIONS **1,203** CITATIONS
SEE PROFILE

Alexey G. Petrunin
Helmholtz-Zentrum Potsdam - Deutsches Ge…
40 PUBLICATIONS **628** CITATIONS
SEE PROFILE

LETTER

doi:10.1038/nature10385

Linking mantle plumes, large igneous provinces and environmental catastrophes

Stephan V. Sobolev[1,2]*, Alexander V. Sobolev[3,4,5]*, Dmitry V. Kuzmin[4,6], Nadezhda A. Krivolutskaya[5], Alexey G. Petrunin[1,2], Nicholas T. Arndt[3], Viktor A. Radko[7] & Yuri R. Vasiliev[6]

Large igneous provinces (LIPs) are known for their rapid production of enormous volumes of magma (up to several million cubic kilometres in less than a million years)[1], for marked thinning of the lithosphere[2,3], often ending with a continental break-up, and for their links to global environmental catastrophes[4,5]. Despite the importance of LIPs, controversy surrounds even the basic idea that they form through melting in the heads of thermal mantle plumes[2,3,6–10]. The Permo-Triassic Siberian Traps[11]—the type example and the largest continental LIP[1,12]—is located on thick cratonic lithosphere[1,12] and was synchronous with the largest known mass-extinction event[1]. However, there is no evidence of pre-magmatic uplift or of a large lithospheric stretching[7], as predicted above a plume head[2,6,9]. Moreover, estimates of magmatic CO_2 degassing from the Siberian Traps are considered insufficient to trigger climatic crises[13–15], leading to the hypothesis that the release of thermogenic gases from the sediment pile caused the mass extinction[15,16]. Here we present petrological evidence for a large amount (15 wt%) of dense recycled oceanic crust in the head of the plume and develop a thermomechanical model that predicts no pre-magmatic uplift and requires no lithospheric extension. The model implies extensive plume melting and heterogeneous erosion of the thick cratonic lithosphere over the course of a few hundred thousand years. The model suggests that massive degassing of CO_2 and HCl, mostly from the recycled crust in the plume head, could alone trigger a mass extinction and predicts it happening before the main volcanic phase, in agreement with stratigraphic and geochronological data for the Siberian Traps and other LIPs[5].

Petrological studies of Siberian Traps and associated alkaline rocks reveal high temperatures (1,600–1,650 °C)[14,17] in their mantle sources. Olivine compositions in samples from lower units of the Norilsk lava section provide evidence that the mantle source of the Siberian Traps was unusually rich in ancient recycled oceanic crust[14], in agreement with earlier predictions[10]. For the main volcanic phase, however, such data were unavailable. Here we report 2,500 new olivine analyses and host-rock compositions for 45 basalts covering the main stages of tholeiitic magmatism in three key localities: the Norilsk area, the Putorana plateau and the Maymecha–Kotuy province (Fig. 1a). Almost all olivine compositions possess significantly higher NiO and FeO/MnO than expected for olivine in peridotite-derived magmas (Fig. 1b, c and Supplementary Fig. 1), suggesting a contribution of melts from pyroxenitic sources[18]. Alternative explanations for these observations seem less plausible (see Methods for discussion). Our interpretation of the olivine compositions implies that the source of the Siberian Traps contained 10–20 wt% recycled oceanic crust (Methods). More specifically, all lavas erupted during the first stage of magmatic activity (Gudchikhinskaya and earlier suites of the Norilsk area) are depleted in heavy rare-earth elements[19,20], indicating residual garnet and derivation within or below the base of thick lithosphere (more than 130 km depth)[14]. The source of Gudchikhinskaya lavas was probably almost entirely pyroxenitic[14] (Fig. 1b–d). Younger magmas are not depleted in heavy rare-earth elements, indicating their formation at shallow depths and marked thinning of the lithosphere. Our calculation suggests that these magmas had a near-constant proportion of pyroxenite-derived melt of about 50% (Fig. 1d and Supplementary Table 1) and were strongly contaminated by the continental crust[20]. Because the main Norilsk section spans less than 1 Myr (ref. 1), it is likely that the lithosphere was thinned in only a few hundred thousand years.

High mantle temperatures over a vast area (Fig. 1a) are consistent with the head of a hot mantle plume[6,9,17]. On the basis of the petrological constraints we develop a thermomechanical model of the interaction of the plume and lithosphere (see Methods). We assume that the plume arrived below the lithosphere at about 253 Myr ago (model time 0), perhaps near the northern border of the Siberian Shield, where the hottest melts (meimechites) erupted[17]. We further assume that the plume head was hot (T_p = 1,600 °C; 250 °C excess temperature) and contained a high content (15 wt%) of recycled oceanic crust. In our two-dimensional model we approximate the plume head by a half-circle of radius 400 km located below cratonic lithosphere of variable thickness corresponding to the margin of the Archean craton (130–250 km of depleted lithosphere and 160–250 km of thermal lithosphere; Fig. 2b and Supplementary Fig. 2).

The arrival of a large and hot mantle plume head at the base of the lithosphere has been predicted[6,21] to cause about 0.8–1 km of broad surface uplift per 100 °C of plume excess temperature. For a purely thermal plume with an excess temperature of 250 °C, we do indeed obtain about 2.0 km of surface uplift (Fig. 2a, red curve). However, if a large fraction (15 wt%) of dense recycled material is present within the plume, its buoyancy is strongly decreased, resulting in little regional uplift (250 m) (Fig. 2a, black curve). Other processes leading to surface subsidence, such as the plume-induced rise of the 670-km phase boundary[22] or the crystallization and evacuation of melts, may easily counteract such a small uplift.

The plume head erodes the lowest part of the thermal lithosphere and rapidly spreads below the more refractory depleted lithosphere (Fig. 2b). Its ascent leads to progressive melting of recycled eclogitic material in the plume and to the formation of reaction pyroxenite, which melts at depths of 130–180 km, well before the peridotite (Fig. 2e). The early, purely pyroxenite-derived, melts yielded the lavas of the Gudchikhinskaya and earlier suites that display the 'garnet signature' (Fig. 1d).

We propose that massive intrusion of the Gudchikhinskaya suite by dykes imposed compressive stress in the upper brittle part of the lithosphere, 'locking' it to the magma transport (Fig. 2b, e shows the moment of 'locking'). After that, the melt could intrude only into the lower

[1]Deutsches GeoForschungsZentrum GFZ, Telegrafenberg, 14473, Potsdam, Germany. [2]O.Yu. Schmidt Institute of the Physics of the Earth, Russian Academy of Sciences, 10 ul. B. Gruzinskaya, Moscow, 123995, Russia. [3]ISTerre, CNRS, University Joseph Fourier, Maison des Géosciences, 1381 rue de la Piscine, BP 53, 38041 Grenoble Cedex 9, France. [4]Max Planck Institute for Chemistry, 27 J.-J.-Becher-Weg, Mainz, 55128, Germany. [5]V. I. Vernadsky Institute of Geochemistry and Analytical Chemistry, Russian Academy of Sciences, 19 ul. Kosygina, Moscow, 119991, Russia. [6]V. S. Sobolev Institute of Geology and Mineralogy, Siberian Branch of Russian Academy of Sciences, 3 prosp. Akad. Koptyuga, Novosibirsk, 630090, Russia. [7]Limited Liability Company 'Norilskgeologiya' Norilsk, PO Box 889, 663330, Russia.

*These authors contributed equally to this work.

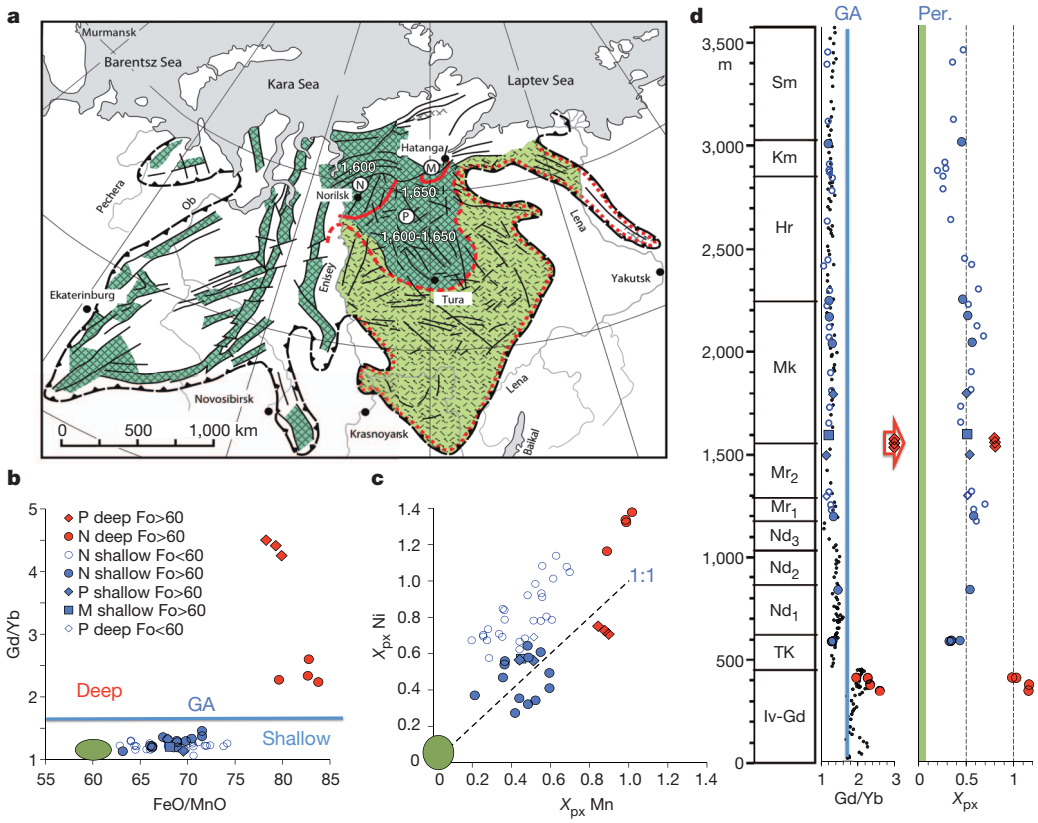

Figure 1 | Petrological constraints. **a**, Geological map of the Siberian Traps[32]. Dark green areas are lavas, light green areas are tuffs. The dashed black line marks the border of the province. Red lines outline areas with different magmatic activities: solid indicates maximal, dashed is moderate, and dotted is minimal. The three studied regions are Norilsk (N), Putorana plateau (P) and Maymecha–Kotuy province (M). White numbers stand for the potential mantle temperature estimated for lavas of the corresponding areas[14,17]. **b**, FeO/MnO ratios of olivine phenocrysts over normalized Gd/Yb ratios of host lavas. The blue line marks the pressure that divides 'deep' lavas depleted in heavy rare-earth elements from 'shallow' lavas. The green oval is the reference for the almost pure shallow peridotitic mantle source and indicates the compositions of olivine and lavas from the mid-ocean ridge (Knipovich Ridge, North Atlantic) with minimum amounts of recycled ocean crust in their sources[18]. All olivines are the averages of the three highest Fo percentages of each sample. GA, garnet in the mantle source. **c**, The proportions of pyroxenite-derived melt in the mixture of pyroxenite-derived and peridotite-derived melts calculated independently of Mn deficiency (X_{px} Mn) and Ni excess (X_{px} Ni) (Methods). **d**, Integrated lava section for Siberian Traps based on the Norilsk section (Supplementary Information). X_{px} is the proportion of pyroxenite-derived melt, calculated as the average of X_{px} Mn and X_{px} Ni for high-forsterite olivines and as X_{px} Mn for low-forsterite olivines, because X_{px} Ni for the latter yields systematic overestimation (Fig. 1c). Small black dots show lavas of the Norilsk section[19]. For abbreviations indicating the lava suites of the Norilsk area and normalization for Dy/Yb ratio, see Supplementary Information. Per, peridotite-derived melt component.

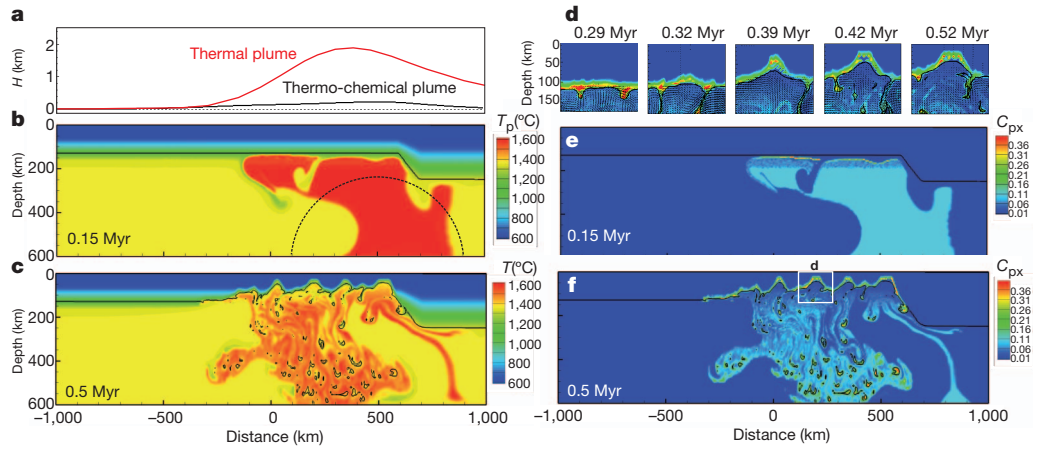

Figure 2 | Model. **a**, Maximum pre-magmatic surface uplift (H) atop a spreading mantle plume with an excess temperature of 250 °C. The red curve corresponds to the purely thermal plume, and the black curve corresponds to a thermo-chemical plume containing 15 wt% of recycled crust. **b**, **c**, Temperature distributions (°C) in the model cross-section at model times of 0.15 Myr (**b**) and 0.5 Myr (**c**). The solid line marks the boundary of the depleted lithosphere, and the dashed half-circle denotes the initial shape of the starting plume. **d**, Snapshots of the plume breaking through the lithosphere in the domain shown by the white rectangle in **f**. Colours show concentrations of the pyroxenitic component in the plume or in the crystallized melt. **e**, **f**, Distribution of the pyroxenite component in the plume (C_{px}) or in the crystallized melt in the model cross-section at model times of 0.15 Myr (**e**) and 0.5 Myr (**f**). The solid line marks the boundary of the depleted lithosphere.

lithosphere (see Methods). The intruding melt cools and crystallizes to dense eclogite. It also strongly heats and weakens the lithosphere, promoting Raleigh–Taylor instabilities[8]. The lower part founders, and the base of the lithosphere is mechanically eroded (Fig. 2c). Enriched in eclogite, the lithospheric material in the boundary layer above the plume escapes to the sides of the plume and then downwards, allowing the plume to ascend (Fig. 2d, f). The plume breaks through the lithosphere in several zones, and in only 100–200 kyr reaches its minimum depth of about 50 km (Fig. 2d and Supplementary Fig. 2). At this level, mafic melts crystallize to a garnet-free assemblage and have a density lower than that of the ambient mantle, thus preventing the formation of Raleigh–Taylor instabilities. This mode of rapid lithosphere destruction does not require regional stretching and matches observations for the Siberian Traps[7,12].

The extent of lithospheric destruction depends, among other factors (Supplementary Information), on the initial density of mantle lithosphere, which is controlled by its composition (Fig. 3a and Supplementary Information). In the case of re-fertilized or moderately depleted mantle lithosphere, the volume of the melt that intrudes into the crust (melt crossing 50 km depth) reaches few per cent of the plume volume (Fig. 3a), which leads to substantial melting of the crust and contamination of basalts. Using the proportion of the magma-to-plume volumes from a two-dimensional model for a three-dimensional plume head with a radius of 400 km, we estimate the volume of the magma intruded into the crust to be $(6–8) \times 10^6$ km^3, which is realistic for the Siberian Traps[1,12].

In agreement with geochemical data, the model predicts that most magma contains about 50% of pyroxenite-derived melt (Fig. 3b, blue curves and symbols) and lack the 'garnet signature' because they are generated at depths of less than 60 km. For the melt generated deeper than 100 km, the model predicts a much higher proportion of pyroxenite melt (75–100%; Fig. 3b, red curves), again in agreement with observations (Fig. 3b, red symbols).

Our model allows us to estimate the volume of CO_2 and HCl gases released from the plume. For these calculations we consider separately the recycled crust and peridotitic components by using data from melt inclusions in olivine in Gudchikhinskaya picrites and mantle peridotite as well as published estimates (Methods). For the composition of recycled crust this yields HCl = 137 p.p.m., S = 135 p.p.m., H_2O = 800 p.p.m. and $CO_2 > 900$ p.p.m. The model predicts that most of the CO_2 and HCl in the recycled-crust component of the plume is extracted during its interaction with the lithosphere (Fig. 4a), and a major part is extracted before the main phase of magmatism. For a three-dimensional plume with a radius of 400 km, the mass of extracted CO_2, which comes mostly from the recycled component of the plume, is more than 170×10^{12} tonnes. This is several times larger than previous estimates[13,15] and also exceeds the maximum estimate of the CO_2 released from the magmatic heating of the coals from the Tunguska basin[15].

Our prediction of the mass of CO_2 extracted from the plume is consistent with the amount of CO_2 released during the Permo-Triassic mass extinction estimated from Ca isotope data[23] (Fig. 4a). Moreover, if we use a $\delta^{13}C$ value of −12‰ for pyroxenite-derived melt as measured in Koolau (Hawaii) basaltic melt for the source dominated by the recycled crust component[24], we can also explain the ^{13}C excursion associated with the main mass-extinction event[23] (Methods). Therefore CO_2 from the plume alone may have triggered the main extinction event. We speculate that low-density and low-viscosity volatiles were the first to penetrate the compressed and mechanically locked crust, triggering the extinction (Fig. 4a, upper axis). Alternatively, a sufficient quantity of gases may have been released before lithospheric locking, together with the deep-sited magmas of pre-Gudchikhinskaya suites, which could also produce metamorphic gases by magmatic heating of the coals and carbonates. This alternative is supported by the recent discovery of coal fly ash in Permian rocks from the Canadian High Arctic immediately before the mass extinction, interpreted as a result of combustion of Siberian coal and organic-rich sediments by flood basalts[25]. In either case, according to our model, the major mass extinction happened before the main phase of flood basalt extrusion. In contrast, most of the CO_2 and other gases released by contact metamorphism of carbon-rich and sulphur-rich sediments, which have been suggested as a trigger for the mass extinction[15,16], would be released during the main phase of magmatism. Precise U–Pb dating of Siberian magmatic units and the Permo-Triassic boundary is required to distinguish between the two hypotheses. Nonetheless, existing geochronological data[26,27] and the presence of abundant pyroclastic rocks underlying lavas of the main magmatic phase[11,19] support the idea that the major mass extinction predated the main phase of magmatism (see Fig. 4a, upper axis). Additional large amounts of gases released from heated sediments[15,16] may have been the cause of ^{13}C excursions during the later phases of the biotic crisis[28].

According to our data and model, the plume also generates a surprisingly large amount of HCl (about 18×10^{12} tonnes; Fig. 4a), mostly

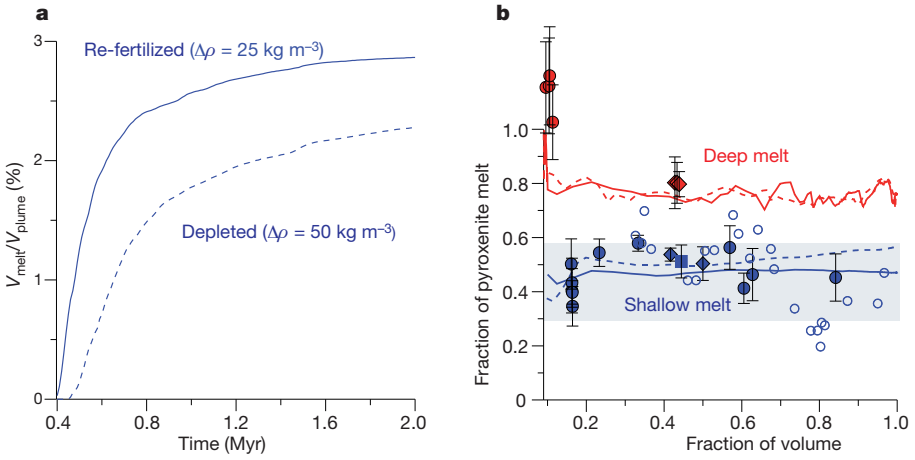

Figure 3 | Model predictions. **a**, Evolution in time of a melt volume crossing the 50-km depth and normalized to the volume of the plume. The solid and dashed curves correspond to the models with re-fertilized lithosphere and moderately depleted lithosphere, respectively. **b**, Plot of the fraction of pyroxenitic component in basalts of the Norilsk cross-section against the fraction of the volume of extruded magmas. The blue colour corresponds to the 'shallow' melts that do not retain a garnet signature; the red colour corresponds to the deep melts that retain a garnet signature. Symbols denote data from olivine compositions; see Fig. 1b for details. Error bars correspond to 1 standard deviation of the mean of pyroxenite-derived melt proportions estimated independently from Ni excess and Mn deficiency of olivine (Methods and Supplementary Table 1). The solid and dashed curves show the modelled average melt compositions with re-fertilized and moderately depleted lithosphere, respectively. The grey rectangle shows the range of variation of the melt compositions predicted by the model.

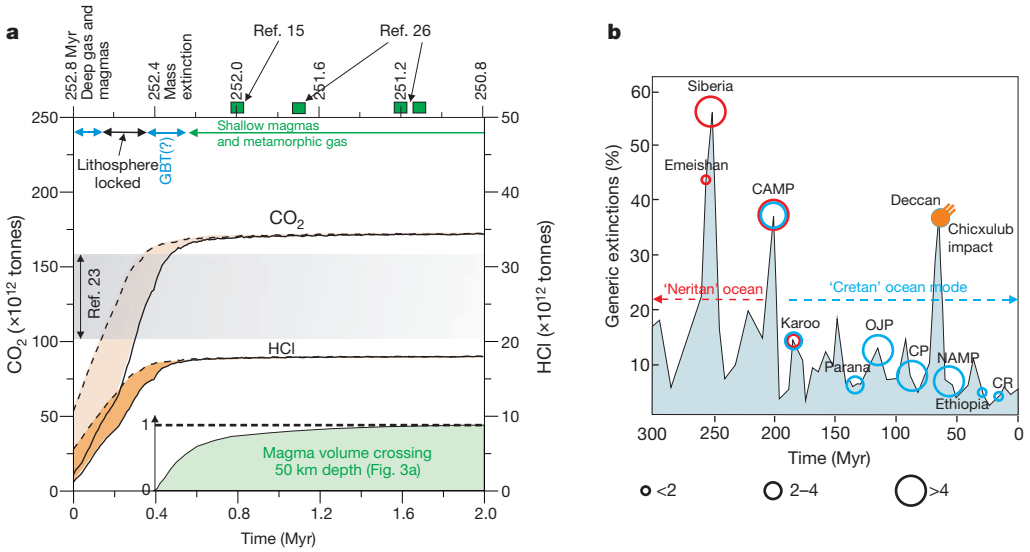

Figure 4 | Production of volatiles and its consequences for mass extinctions. **a**, Plot of modelled CO_2 (left axis) and HCl (right axis) amounts extracted from the plume against model time (lower axis). Solid curves show the minimum estimate and dashed curves the maximum estimate of CO_2 and HCl extracted from the plume (Methods). The grey rectangle shows the estimated range of the released CO_2 during the Permo-Triassic mass extinction[23]. The green area shows time dependence of the normalized volume of the magma crossing the 50-km depth, calculated for the re-fertilized lithosphere (Fig. 3a). On the top axis we show geological time and a possible model for triggering the Permo-Triassic mass extinction. GBT, gases break through. Also shown is U–Pb dating of the extinction event[27] and U–Pb dating of main-phase Siberian basalts[26] and intrusions[15]. **b**, Plot of mass extinction intensity (light blue field) with major LIPs (circles) against geological time (modified from ref. 33), together with the timing of different ocean modes[30]. Circle colours denote the timing of LIPs relative to ocean modes: blue, 'Cretan' mode; red 'Neritan' mode; blue and red together, transition mode. The scale of circle sizes is in millions of cubic kilometres. CAMP, Central Atlantic Magmatic Province; NAMP, Northern Atlantic Magmatic Provinces, OJP, Ontong Java; CP, Caribbean Plateaux; CR, Columbian River basalts.

also derived from the recycled component. This quantity of toxic HCl must have been extremely damaging for the terrestrial species and was also sufficient to trigger deadly instability of the stratospheric ozone layer[29].

By accepting our viewpoint that degassing of the plume, rather than thermogenic gases from sediments, triggered the biotic crises, we lose an elegant explanation of why the Siberian LIP was so much more damaging to biota than other LIPs of comparable size (Karoo, Parana and North Atlantic) that extruded through other types of sediment or granitic rock[15,16]. An alternative explanation is based on the correlation of the intensity of mass extinctions with the age of Phanerozoic LIPs (Fig. 4b), a relationship that can be explained by the temporally different response of the ocean to acidification by the large amounts of released CO_2 (refs 23, 30). In contrast to the pre-Mid-Mesozoic 'Neritan' ocean, the more recent 'Cretan' ocean was buffered against acidification by deep-sea unlithified carbonate sediments and was thus much more resistant to acidification[23,30]. Therefore, CO_2 degassing of a pre-Mid-Mesozoic LIP caused much more severe ocean acidification and mass extinction than later LIPs (Fig. 4b). The only exception is the Deccan LIP and the contemporaneous mass extinction at 65.5 Myr ago; however, in this case the Chicxulub impact was an additional contributing factor[31].

Numerical tests (Supplementary Figs 4–6) suggest that rapid lithospheric destruction associated with melting in the heads of thermochemical plumes is valid for the large range of plume parameters and lithospheric thicknesses, and therefore may apply not only to the Siberian Traps but also to other LIPs. An absence of prominent pre-magmatic uplift does not argue against a plume origin of LIPs, but may instead point to a high content of recycled crust within the plume. In such cases, other parameters being equal, the model predicts that eclogite-rich plumes caused the most extensive delamination and thinning of the lithosphere, thus best preparing it for a possible break-up. They also produced the strongest volcanism and led to the most marked climatic consequences.

Another suggestion of our model—that major mass extinctions are triggered by degassing of plume magmas that predate the main magmatic phase—also seems to be consistent with the observations for many LIPs[5], implying that gas output from plume heads may be much larger than previously thought.

METHODS SUMMARY

We report new data on 45 representative olivine-bearing samples of Siberian flood basalts from the Norilsk, Putorana and Maimecha–Kotui regions (Supplementary Tables 1 and 3). The bulk rocks were crushed, melted and analysed for major and trace elements with an electron probe microanalyser (EPMA) and by laser ablation inductively coupled plasma mass spectrometry (LA-ICP-MS) at the Max Planck Institute for Chemistry in Mainz, Germany. Olivine phenocrysts (about 2,500 analyses) were analysed by EPMA with a special high-precision protocol[18] at the Max Planck Institute for Chemistry. Using this new information and published approaches we estimated the amount of recycled oceanic crust in the sources of basalts and their potential temperatures, and discuss possible alternative models of the source compositions. We further estimate the amounts of H_2O, Cl, S and CO_2 in the recycled oceanic crust and develop a model of its degassing during plume–lithosphere interaction.

We model the thermomechanical interaction of the plume and lithosphere by numerically solving a coupled system of momentum, mass and energy conservation equations in two dimensions. We employ nonlinear temperature and stress-dependent elasto-visco-plastic rheology, consider pressure-dependent and temperature-dependent melting of a heterogeneous mantle and employ simple models of melt transfer and extraction of volatiles.

Full Methods and any associated references are available in the online version of the paper at www.nature.com/nature.

Received 17 February; accepted 26 July 2011.

1. Reichow, M. K. *et al.* The timing and extent of the eruption of the Siberian Traps large igneous province: implications for the end-Permian environmental crisis. *Earth Planet. Sci. Lett.* **277,** 9–20 (2009).
2. White, R. & McKenzie, D. Magmatism at rift zones—the generation of volcanic continental margins and flood basalts. *J. Geophys. Res. Solid Earth Planets* **94,** 7685–7729 (1989).
3. Garfunkel, Z. Formation of continental flood volcanism—the perspective of setting of melting. *Lithos* **100,** 49–65 (2008).
4. Courtillot, V. E. & Renne, P. R. On the ages of flood basalt events. *C. R. Geosci.* **335,** 113–140 (2003).
5. Wignall, P. B. Large igneous provinces and mass extinctions. *Earth Sci. Rev.* **53,** 1–33 (2001).
6. Campbell, I. H. & Griffiths, R. W. Implications of mantle plume structure for the evolution of flood basalts. *Earth Planet. Sci. Lett.* **99,** 79–93 (1990).

7. Czamanske, G. K., Gurevitch, A. B., Fedorenko, V. & Simonov, O. Demise of the Siberian plume: paleogeographic and paleotectonic reconstruction from the prevolcanic and volcanic record, north-central Siberia. *Int. Geol. Rev.* **40,** 95–115 (1998).
8. Elkins-Tanton, L. T. & Hager, B. H. Melt intrusion as a trigger for lithospheric foundering and the eruption of the Siberian flood basalts. *Geophys. Res. Lett.* **27,** 3937–3940 (2000).
9. Richards, M. A., Duncan, R. A. & Courtillot, V. E. Flood basalts and hot-spot tracks—plume heads and tails. *Science* **246,** 103–107 (1989).
10. Cordery, M. J., Davies, G. F. & Campbell, I. H. Genesis of flood basalts from eclogite-bearing mantle plumes. *J. Geophys. Res. Solid Earth* **102,** 20179–20197 (1997).
11. Sobolev, V. S. *Petrology of Siberian Traps* (*Transactions of All-Union Arctic Institute*, vol. 43) (Glavnogo Upravleniaya Sevmorputi, 1936).
12. Dobretsov, N. L., Kirdyashkin, A. A., Kirdyashkin, A. G., Vernikovsky, V. A. & Gladkov, I. N. Modelling of thermochemical plumes and implications for the origin of the Siberian traps. *Lithos* **100,** 66–92 (2008).
13. Self, S., Widdowson, M., Thordarson, T. & Jay, A. E. Volatile fluxes during flood basalt eruptions and potential effects on the global environment: a Deccan perspective. *Earth Planet. Sci. Lett.* **248,** 518–532 (2006).
14. Sobolev, A. V., Krivolutskaya, N. A. & Kuzmin, D. V. Petrology of the parental melts and mantle sources of Siberian trap magmatism. *Petrology* **17,** 253–286 (2009).
15. Svensen, H. *et al.* Siberian gas venting and the end-Permian environmental crisis. *Earth Planet. Sci. Lett.* **277,** 490–500 (2009).
16. Ganino, C. & Arndt, N. T. Climate changes caused by degassing of sediments during the emplacement of large igneous provinces. *Geology* **37,** 323–326 (2009).
17. Sobolev, A. V., Sobolev, S. V., Kuzmin, D. V., Malitch, K. N. & Petrunin, A. G. Siberian meimechites: origin and relation to flood basalts and kimberlites. *Russ. Geol. Geophys.* **50,** 999–1033 (2009).
18. Sobolev, A. V. *et al.* The amount of recycled crust in sources of mantle-derived melts. *Science* **316,** 412–417 (2007).
19. Fedorenko, V. A. *et al.* Petrogenesis of the flood-basalt sequence at Noril'sk, North Central Siberia. *Int. Geol. Rev.* **38,** 99–135 (1996).
20. Wooden, J. L. *et al.* Isotopic and trace-element constraints on mantle and crustal contributions to Siberian continental flood basalts, Norilsk Area, Siberia. *Geochim. Cosmochim. Acta* **57,** 3677–3704 (1993).
21. Farnetani, C. G. & Richards, M. A. Numerical investigations of the mantle plume initiation model for flood-basalt events. *J. Geophys. Res. Solid Earth* **99,** 13813–13833 (1994).
22. Leng, W. & Zhong, S. J. Surface subsidence caused by mantle plumes and volcanic loading in large igneous provinces. *Earth Planet. Sci. Lett.* **291,** 207–214 (2010).
23. Payne, J. L. *et al.* Calcium isotope constraints on the end-Permian mass extinction. *Proc. Natl Acad. Sci. USA* **107,** 8543–8548 (2010).
24. Hauri, E. SIMS analysis of volatiles in silicate glasses. 2. Isotopes and abundances in Hawaiian melt inclusions. *Chem. Geol.* **183,** 115–141 (2002).
25. Grasby, S. E., Sanei, H. & Beauchamp, B. Catastrophic dispersion of coal fly ash into oceans during the latest Permian extinction. *Nature Geosci.* **4,** 104–107 (2011).
26. Kamo, S. L. *et al.* Rapid eruption of Siberian flood-volcanic rocks and evidence for coincidence with the Permian–Triassic boundary and mass extinction at 251 Ma. *Earth Planet. Sci. Lett.* **214,** 75–91 (2003).
27. Mundil, R., Palfy, J., Renne, P. R. & Black, P. The Triassic timescale: new constraints and a review of geochronological data. *Geol. Soc. Lond. Spec. Pub.* **334,** 41–60 (2010).
28. Payne, J. L. & Kump, L. R. Evidence for recurrent Early Triassic massive volcanism from quantitative interpretation of carbon isotope fluctuations. *Earth Planet. Sci. Lett.* **256,** 264–277 (2007).
29. Beerling, D. J., Harfoot, M., Lomax, B. & Pyle, J. A. The stability of the stratospheric ozone layer during the end-Permian eruption of the Siberian Traps. *Phil. Trans. R. Soc. Lond. A* **365,** 1843–1866 (2007).
30. Ridgwell, A. A mid Mesozoic revolution in the regulation of ocean chemistry. *Mar. Geol.* **217,** 339–357 (2005).
31. Schulte, P. *et al.* The Chicxulub asteroid impact and mass extinction at the Cretaceous–Paleogene Boundary. *Science* **327,** 1214–1218 (2010).
32. Masaitis, V. L. Permian and Triassic volcanism of Siberia: problems of dynamic reconstructions [in Russian]. *Zapiski Vsesouznogo Mineralogicheskogo Obshestva* **112,** 412–425 (1983).
33. White, R. V. & Saunders, A. D. Volcanism, impact and mass extinctions: incredible or credible coincidences? *Lithos* **79,** 299–316 (2005).

Supplementary Information is linked to the online version of the paper at www.nature.com/nature.

Acknowledgements S.V.S. and A.V.S. are especially grateful to Vladimir Stepanovich Sobolev, who excited their interest in the origin of the Siberian Traps. We thank G. A. Fedorenko for providing data on the Norilsk lavas and for discussions; N. Groschopf for help in managing the electron probe microanalyser; O. Kuzmina, N. Svirskaya and T. Shlichkova for sample preparation; P. Cardin, N. Dobretsov, E. Galimov, C. Herzberg, A. Hofmann, L. Kogarko, H.-C. Nataf, J. Payne, Y. Podladchikov, I. Ryabchikov, A. Turchyn and G. Wörner for discussions; and P. Kelemen for comments. S.V.S. thanks the Deutsche Forschungsgemeinschaft (DFG) SPP 1375 SAMPLE (SO 425/4) for support. The study by A.V.S. was funded by the Agence Nationale de la Recherche, France (Chair of Excellence Grant ANR-09-CEXC-003-01) and partly supported by a Gauss Professorship in Göttingen University, Germany, the Russian Foundation for Basic Research (09-05-01193a), a Russian President grant for leading Russian scientific schools (НШ-3919.2010.5) and an Earth Sciences Department of Russian Academy Grants.

Author Contributions S.V.S. and A.V.S. provided major contributions to thermomechanical (S.V.S.) and petrological (A.V.S.) modelling, to the interpretation of data and to the writing of the paper. N.A.K. provided geological background and contributed to interpretation. A.G.P. contributed to the thermomechanical modelling at an initial stage. N.T.A. contributed to interpretation and writing of the paper. D.V.K. processed samples and performed the measurements. N.A.K., V.A.R. and Y.R.V. provided carefully selected samples. All authors contributed intellectually to the paper.

Author Information Reprints and permissions information is available at www.nature.com/reprints. The authors declare no competing financial interests. Readers are welcome to comment on the online version of this article at www.nature.com/nature. Correspondence and requests for materials should be addressed to S.V.S. (stephan@gfz-potsdam.de) or A.V.S. (alexander.sobolev@ujf-grenoble.fr).

METHODS

Samples. The samples studied and their localities are described in Supplementary Information.

Analytical methods. Olivine grains were manually separated from crushed lavas, then mounted and polished in epoxy. The compositions of olivine were analysed with an EPMA on a Jeol JXA 8200 SuperProbe at the Max Planck Institute for Chemistry (Mainz, Germany) at an accelerating voltage of 20 kV and a beam current of 300 nA, following a special procedure which allows 20–30 p.p.m. (2σ error) precision and accuracy for Ni, Ca, Mn, Al, Ti, Cr and Co, and 0.02 mol% accuracy for the forsterite component in olivine[18].

Bulk rocks were crushed, melted to glass[34] and then mounted and polished in epoxy. Major and trace elements were also determined by EPMA at the Max Planck Institute for Chemistry. Major-element abundances in glasses were measured at an accelerating voltage of 15 kV and a beam current of 12 nA with a reference sample of natural basaltic glass USNM111240/52 (VG2)[35], with a relative error of 1–2%. LA-ICP MS was used to determine trace elements in glasses of melt inclusions and in olivines, on an ELEMENT-2, Thermo Scientific mass spectrometer with a UP-213 New Wave Research solid-phase laser at the Max Planck Institute for Chemistry, with reference to the KL-2G and NIST 612 standard samples of basaltic glass[36].

Proportions of pyroxenite-derived melt and recycled crust. We interpret excessive Ni and deficient Mn concentrations in Siberian olivine phenocrysts relative to olivine in peridotite-derived melt as a result of the contribution of olivine free pyroxenite lithology in their source[18,37–39]. The alternative explanations of this phenomenon are discussed briefly in the next section. Relative proportions of pyroxenite and peridotite derived melts were estimated from MnO/FeO (X_{px} Mn) and NiO × FeO/MgO (X_{px} Ni) ratios[38] for each sample, using the average composition of most magnesian olivines (defined by olivines with Fo within 3 mol% from a maximum Fo).

The amount of recycled crust in the plume is linked to the proportion of pyroxenite-derived melt by the degree of melting of the eclogite component, the amount of eclogite-derived melt needed to produce hybrid pyroxenite from peridotite, and the degrees of melting of peridotite and pyroxenite[18,39]. We calculated the amount of recycled crust in the Siberian plume using the approach described previously[18] and their equation S3, and the following assumptions: a maximum degree of melting of eclogite and pyroxenite of 60%; an average proportion of pyroxenite-derived melt in shallow magmas of 46% (Supplementary Table 1); and melting of peridotite at 50 km depth. The amounts of recycled crust are 10% and 20% for 10% and 25% melting of peridotite, respectively.

Alternative explanations of the unusual olivine composition. Alternative explanations of high Ni/Mg and FeO/MnO ratios in olivine include: (1) effect of clinopyroxene crystallization, (2) an underestimated temperature effect on olivine-melt partition of Ni, and (3) contribution of core material to the mantle source. None of these alternatives require a significant role of olivine-free pyroxenite in the mantle source. In addition there are different models for the pyroxenite origin, which may affect our estimation of proportions of pyroxenite in the Siberian plume. These include (4) solid-state reaction of peridotite and recycled crust in the lower mantle and (5) partial reaction between eclogite-derived melt and peridotite. Below we briefly discuss these alternatives.

1. Crystallization of clinopyroxene together with olivine may increase both Ni/Mg and Fe/Mn ratios in olivine. This effect could be particularly important for the low magnesian evolved olivine. However clinopyroxene crystallization can be recognized by low Ca in olivine. In Supplementary Information we show that this is an unlikely situation for most studied olivines, which do not show a significant decrease in Ca concentrations. In particular, early clinopyroxene crystallization cannot explain the composition of the olivines from picrites of the Gudchikhinskaya formation and the Ayan river, which are extremely rich in Ni and deficient in Mn. In addition, melt inclusions in the former[14] and olivines in the latter (Supplementary Table 3) do not indicate early clinopyroxene crystallization. We conclude that the fractionation of clinopyroxene could not have produced the observed anomalies in the olivine compositions.

2. An underestimated temperature effect on olivine-melt partition coefficient, if present, may increase Ni concentration in the shallow olivine compared with olivine in the deep source as a result of temperature difference between the sites of generation and crystallization. This issue has been discussed previously[37,39], where it was shown that any temperature effect additional to the compositional one considered in the model of Ni partitioning between melt and olivine used in this study[40] is too small to explain the extent of Ni excess observed in Siberian olivines.

3. The contribution of core material to increase Ni/Mg (ref. 41) and Fe/Mn (ref. 42) ratios has been discussed previously[18], where it was shown that this explanation is highly unlikely because of a lack of correlation between Ni excess and high Co concentrations in the olivines.

4. The solid-state reaction between recycled crust and peridotite in the lower mantle may produce pyroxenite with a composition much closer to that of peridotite, which in the upper mantle will be transformed to olivine-bearing pyroxenite[37]. If this lithology exists, it could potentially be the source of parental melts of typical Siberian basalts. However, olivine-bearing lithologies could not be the source of deep-sourced lavas such as the Gudchikhinskaya formation and Ayan river picrites, whose olivine compositions demonstrate derivation from a dominating olivine-free source. In addition, solid-state reactions of the type envisaged in ref. 37 will be limited by slow volume diffusion in the mantle[43], whereas the production of reaction olivine-free pyroxenite will be restricted only by melt percolation velocity[18,39].

5. Incomplete reaction between eclogite-derived melt and peridotite may produce olivine-bearing lithologies[44], which could be potential sources of the parental melts of typical Siberian traps. However, these olivine-bearing lithologies cannot produce Siberian deep-sourced magmas (see above).

We conclude that although we cannot fully exclude some of proposed alternatives, our explanation of the olivine compositions is based on solid grounds and seems the most plausible.

Potential temperatures. The published potential temperature of 1,540 °C for the source of Gudchikhinskaya magmas[14] has been corrected for the effect of 40% melting of pyroxenitic source[17], the amount of pyroxenite in the plume (15%) and the latent heat of melting[45]. The value obtained is about 1,600 °C. Potential temperatures for the Maimecha–Kotuy province[17] and the Putorana plateau[46] (see Fig. 1a) were obtained for magmas strongly enriched in highly incompatible elements. These magmas originated at low degrees of melting and thus were not corrected for the melting effect.

Amount of volatile elements. The concentrations of volatile elements in the recycled oceanic crust in the Siberian plume were constrained using the compositions of inclusions of uncontaminated melt in early olivine phenocrysts from Gudchikhinskaya magmas. For these magmas it was shown from both olivine and melt compositions that they probably represent the melting of a pure pyroxenitic source[14]. Inclusions in olivine from these magmas have been shown to represent primary melts[14] and thus their concentrations of Cl, S and H_2O can be used to estimate the contents of these volatiles in the mantle source. For the composition of source eclogite, this yields the following values[14,17]: Cl = 137 p.p.m., S = 135 p.p.m. and H_2O = 800 p.p.m., after normalization of the values to K. In the deep mantle, these amounts of Cl, S and H_2O could reside in chloride[47], sulphide, and garnet or pyroxene respectively. In contrast with Cl, S and H_2O, the amount of CO_2 in relatively shallow melts does not represent the primary concentration, because of almost complete degassing at high pressures. Thus for an assessment of CO_2 in the recycled oceanic crust we use global estimations of 3,000 p.p.m. CO_2 for the bulk 7-km-thick oceanic crust and its maximum outgassing rate through arc volcanism of 70% (ref. 48). This gives a conservative minimum estimate of 900 p.p.m. CO_2 in the deeply recycled oceanic crust. The maximum estimate would be about 1,800 p.p.m. using the same initial bulk concentrations of CO_2 and minimal outgassing of 40% (ref. 48). In the deep mantle this amount of CO_2 could reside in carbonates or diamond[47]. For our model we use the minimum conservative estimate of CO_2 = 900 p.p.m.

Thermo-mechanical numerical technique. We use a fully coupled thermo-mechanical formulation for the system of momentum, mass and energy conservation equations in two dimensions with nonlinear temperature and stress-dependent elasto-visco-plastic rheology, described in detail in ref. 49 (for parameters and procedure for calculating density, see Supplementary Information). Equations are solved numerically using the explicit Lagrangean FEM technique LAPEX2D (ref. 50) based on a FLAC algorithm (prototype described in ref. 51) combined with a particle-in-cell approach. All time-dependent fields including full stress tensor are stored at particles.

Melting models. We use a simplified model for batch melting of four components: peridotite, pyroxenite and two eclogites formed through the crystallization of peridotitic and pyroxenitic melts, respectively. Melting temperatures are defined as follows: for peridotite we use the dry batch melting model[52]; for pyroxenite we use the following relation from experiments[18] for dry batch melting of pyroxenite:

$$T_m^{Px} = 976 + 12.3P - 0.051P^2 + 663.8X - 611.4X^2$$

where P is pressure in kbars, T is potential temperature in °C and X is degree of melting, $0 < X < 0.55$.

For eclogite of both types (peridotite-derived or pyroxenite-derived) we use the following relations approximating experiments[53] for dry batch melting of eclogite at 50% melting:

$$T_m^e = 1173.4 + 5.78P$$

at $P < 55$ kbar, and

$$T_m^e = -237.5 + 48.0P - 0.3P^2$$

at $55 \leqslant P < 80$ kbar.

The melting for each finite element is organized sequentially, beginning with the component with the lowest melting temperature (usually eclogite), then usually pyroxenite and finally peridotite. If the current temperature (T) in a finite element exceeds the melting temperature (T_m) of the component that exists in this element, than a certain amount of melt (dC_m) is generated that lowers the current temperature to the melting temperature, $dC_m = (T - T_m)C_p/(\Delta S_m T)$, where C_p is heat capacity and ΔS_m is entropy of melting, set to 1,200 J kg^{-1} K^{-1} and 400 J kg^{-1} K^{-1}, respectively, for all components.

Model for melt transfer. We assume that melt transfer within the melting domain occurs much faster than the Raleigh–Taylor instability develops in the lithosphere. This assumption holds if the velocity of melt transfer (V_m) is much higher than H/τ, where H is the typical distance of melt transfer and τ is typical time of Raleigh–Taylor instability. With values of $H < 50$ km and $\tau \approx 50{,}000$ years (see Supplementary Fig. 2), this assumption is valid if V_m is much higher than 1 m yr^{-1}. In reality, V_m is at least tenfold higher in the upper mantle regions where intensive melting occurs[54].

If present, the entire melt is assumed to move rapidly upwards within the domain where the local temperature is higher than the melting temperature. As usual for melt porous flow, we also assume that it is thermally equilibrating at each element. In practice, at every nth calculation time-step, for every element we check the melting condition and move the entire volume of melt (if present) one element upwards, recalculating the temperature of that element according to the local energy conservation law.

For the melt in the uppermost elements of the melting domain, we consider two transfer modes. First we consider a mode that mimics transfer through fractures: in this case, a fraction or the entire melt is assumed to move to the surface; in practice it is just taken out from the model. Second, we consider a mode of mechanically locked lithosphere: in this case the entire melt from each uppermost element of the melting zone is moved to, and evenly distributed between, K elements in the column just above it (usually we take $K = 4$) and is assumed to crystallize. Simultaneously, the rheology of melt-accepting lithospheric elements is switched from 'dry' to 'wet' olivine rheology if the crystallized melt content exceeds some critical value (we take this value as 1%). The temperature and composition of the accepting elements are recalculated according to the local energy and mass conservation laws.

Extraction of volatiles. We consider two endmember models for the extraction of volatiles. In the first model we assume that CO_2 and HCl are fully extracted from the plume if the temperature approaches that of the carbonatite solidus[55]. This model gives an upper bound for melt mobility, assuming that melts produced by an infinitely low degree of melting can move out of the plume. In the second model we assume that CO_2 and HCl are fully extracted from both peridotitic and pyroxenitic components only if 1% melting is achieved. This model gives lower boundary for melt mobility, assuming that only 1% carbonate–silicate melts can move out of the plume. For both models we assume a concentration of HCl in recycled crust of 137 p.p.m. derived from melt inclusions in olivine, no HCl in the peridotitic component and minimum conservative estimates of CO_2 content in both recycled crust (900 p.p.m.) and plume peridotite (70 p.p.m.) (see above).

Expected mode of motion of volatiles in the lithosphere. Melt from the plume is trapped and crystallizes in the lithosphere; it then returns to the mantle as the lithosphere founders. The volatiles extracted by melting of the plume are released as the melt crystallizes because host phases are not stable at the high temperatures at the base of the lithosphere. They migrate upwards, then react and are fixed in carbonates or chlorides in the cooler upper part of the lithosphere. Continuous upward migration of high-temperature isotherms then decomposes these phases, promoting further displacement of the volatile front ahead of the basalt-melting front. According to our model, more than 70% of the mafic magmas generated in the plume crystallized to eclogites and subsided back into the mantle as the densified lithosphere foundered; less than 30% were intruded into the crust. However, almost all carbonatite melts traversed the lithosphere and crust, because the temperature of the detached blocks was significantly higher than the melting temperature of carbonatite. It is therefore likely that a significant part of the volatiles released from the plume finally reached the surface, promoting explosive eruptions, which are very common in the early stage of Siberian Traps[11,19] and other LIPs, that is, Emeishan flood basalts[56]. Note that the volatiles that were initially stored in the minerals of the destructed portions of the lithosphere should be also melted out and could finally reach the surface as well.

Why output of volatiles from LIPs could be drastically underestimated. The amount of volatiles released was previously estimated using only the volume of extruded magmas or magmas intruded into the shallow crust. In these studies were disregarded the magmas that crystallized in the deep crust and, more importantly, the much larger volumes of magmas that we propose were involved in the destruction of the lithosphere and never reached the crust, although most of the volatiles extracted from them probably did (see above). Additionally, the recycled crust component of the plume, which contains much more volatiles than the peridotitic component, was not previously considered in the balance calculation.

Estimation of ^{13}C excursion. The ^{13}C-isotope change due to the released CO_2 (considered to be instantaneous) can be estimated from a simple mass-balance equation[38]. According to our model, about 172×10^{12} tonnes of CO_2 is released from the plume—about 70% from recycled crust and the remaining 30% from peridotite. Assuming that $\delta^{13}C = -12‰$ for crust-derived CO_2 (ref. 24) and $\delta^{13}C = -5‰$ for peridotite-derived CO_2, we obtain an average isotopic composition of the plume-released carbon of $\delta^{13}C = -9.9‰$. Assuming $\delta^{13}C = 3.6‰$ for the initial carbon isotope composition and 300×10^{12} tonnes of CO_2 (or 82×10^{12} tonnes of C)[23] for the Late Permian CO_2 reservoir, we estimate that the magnitude of the carbon isotope excursion was 4.9‰ if all plume-released gases migrated to the surface, and 3.5‰ if only half of them arrived. Both numbers are well within the range of reported values for the Permian–Triassic excursion[57].

34. Stoll, B. *et al.* An automated iridium-strip heater for LA-ICP-MS bulk analysis of geological samples. *Geostand. Geoanal. Res.* **32,** 5–26 (2008).
35. Jarosevich, E. J., Nelen, J. A. & Norberg, J. A. Reference sample fro electron microprobe analysis. *Geostand. Newsl.* **4,** 43–47 (1980).
36. Jochum, K. P. *et al.* The preparation and preliminary characterisation of eight geological MPI-DING reference glasses for in-site microanalysis. *Geostand. Newsl.* **24,** 87–133 (2000).
37. Herzberg, C. Identification of source lithology in the Hawaiian and Canary Islands: implications for origins. *J. Petrol.* **52,** 113–146 (2011).
38. Sobolev, A. V., Hofmann, A. W., Brugmann, G., Batanova, V. G. & Kuzmin, D. V. A quantitative link between recycling and osmium isotopes. *Science* **321,** 536 (2008).
39. Sobolev, A. V., Hofmann, A. W., Sobolev, S. V. & Nikogosian, I. K. An olivine-free mantle source of Hawaiian shield basalts. *Nature* **434,** 590–597 (2005).
40. Beattie, P., Ford, C. & Russell, D. Partition coefficients for olivine-melt and orthopyroxene-melt systems. *Contrib. Mineral. Petrol.* **109,** 212–224 (1991).
41. Ryabchikov, I. D. High NiO content in mantle-derived magmas as evidence for material transfer from the Earth's core. *Dokl. Earth Sci.* **389,** 437–439 (2003).
42. Humayun, M., Qin, L. P. & Norman, M. D. Geochemical evidence for excess iron in the mantle beneath Hawaii. *Science* **306,** 91–94 (2004).
43. Holzapfel, C., Chakraborty, S., Rubie, D. D. & Frost, D. J. Effect of pressure on Fe-Mg, Ni and Mn diffusion in $(Fe_xMg_{1-x})_2SiO_4$ olivine. *Phys. Earth Planet. Inter.* **162,** 186–198 (2007).
44. Kelemen, P. B., Hart, S. R. & Bernstein, S. Silica enrichment in the continental upper mantle via melt/rock reaction. *Earth Planet. Sci. Lett.* **164,** 387–406 (1998).
45. Manglik, A. & Christensen, U. R. Effect of lithospheric root on decompression melting in plume–lithosphere interaction models. *Geophys. J. Int.* **164,** 259–270 (2006).
46. Ryabchikov, I. D., Solovova, I. P., Ntaflos, T., Buchl, A. & Tikhonenkov, P. I. Subalkaline picrobasalts and plateau basalts from the Putorana plateau (Siberian continental flood basalt province). II. Melt inclusion chemistry, composition of 'primary' magmas and *P–T* regime at the base of the superplume. *Geochem. Int.* **39,** 432–446 (2001).
47. Safonov, O. G., Kamenetsky, V. S. & Perchuk, L. L. Links between carbonatite and kimberlite melts in chloride–carbonate–silicate systems: experiments and application to natural assemblages. *J. Petrol.* **52,** 1307–1331 (2011).
48. Dasgupta, R. & Hirschmann, M. M. The deep carbon cycle and melting in Earth's interior. *Earth Planet. Sci. Lett.* **298,** 1–13 (2010).
49. Sobolev, S. V. & Babeyko, A. Y. What drives orogeny in the Andes? *Geology* **33,** 617–620 (2005).
50. Babeyko, A. Y., Sobolev, S. V., Trumbull, R. B., Oncken, O. & Lavier, L. L. Numerical models of crustal scale convection and partial melting beneath the Altiplano-Puna plateau. *Earth Planet. Sci. Lett.* **199,** 373–388 (2002).
51. Poliakov, A. N., Cundall, P. A., Podladchikov, Y. Y. & Lyakhovsky, V. A. in *Flow and Creep in the Solar System: Observations, Modelling and Theory* (eds Stone, D. B. & Runcorn, S. K.) 175–195 (Kluwer Academic, 1993).
52. Katz, R. F., Spiegelman, M. & Langmuir, C. H. A new parameterization of hydrous mantle melting. *Geochem. Geophys. Geosyst.* **4,** doi:10.1029/2002gc000433 (2003).
53. Spandler, C., Yaxley, G., Green, D. H. & Rosenthal, A. Phase relations and melting of anhydrous K-bearing eclogite from 1200 to 1600 degrees C and 3 to 5 GPa. *J. Petrol.* **49,** 771–795 (2008).
54. Kelemen, P. B., Hirth, G., Shimizu, N., Spiegelman, M. & Dick, H. J. B. A review of melt migration processes in the adiabatically upwelling mantle beneath oceanic spreading ridges. *Phil. Trans. R. Soc. Lond. A* **355,** 283–318 (1997).
55. Dasgupta, R. & Hirschmann, M. M. Effect of variable carbonate concentration on the solidus of mantle peridotite. *Am. Mineral.* **92,** 370–379 (2007).
56. Wignall, P. B. *et al.* Volcanism, mass extinction and carbon isotope fluctuations in the Middle Permian of China. *Science* **324,** 1179–1182 (2009).
57. Retallack, G. J. & Jahren, A. H. Methane release from igneous intrusion of coal during late Permian extinction events. *J. Geol.* **116,** 1–20 (2008).

SUPPLEMENTARY INFORMATION

doi:10.1038/nature10385

Samples description

Studied samples are olivine phyric, olivine-plagioclase phyric or aphyric basalts and rarely picrites from outcrops or drill core of lava flows (most samples), and outcrops of dykes (few samples) see Supplementary Table S1. They contain visually fresh olivine phenocrysts, microphenocrysts or olivine-pyroxene intergrowths and were carefully selected from lavas from Norilsk area, Putorana plateau and Maymecha-Kotuy province.

Norilsk area. We studied samples from most lava units of the Norilsk section, covering most parts of the region[14,19,58,59]. Samples were carefully located relative to the lower boundaries of the units and were placed within the integrated lava section of Siberian traps using this information and absolute positions of unit boundaries after Fedorenko et al, 1996 ref(*19*). Abbreviations at Fig. 1D indicate the following lava suites of the Norilsk area placed in the order of decreasing age: Iv-Ivakinskaya, Gd-Gudchikhinskaya, Tk-Tuklonskaya, Nd-Nadezhdinskaya, Mr-Morangovskaya, Mk-Mukulaevskaya, Hr-Haerlakhskaya, Km-Kumginskaya, Sm-Samoedskaya. $(Gd/Yb)_n$ indicates the element ratio normalized to the primitive mantle composition[60]. We also studied olivine phyric basaltic dykes (samples 22-12 and 22-6), cutting the upper Mukulaevskaya suite and thus representing any of upper units from Hr to Sm.

Putorana plateau. Studied samples came from collection of V. Nesterenko[61-64] and Y. Vasiliev (picrites of Ayan river)[65]. We estimated approximate positions of studied samples in the integrated lava section (Fig 1D) using data reported in ref(*19, 61*).

Maymecha-Kotuy province. Most lavas of this province are highly alkaline[66,67] and are not discussed in this paper. Here we report olivine compositions from only one sample, which represents the major type of voluminous tholeiitic lavas from the Maymecha-Kotuy province[68]. It is similar in composition to the predominant type of Norilsk and Putorana basalts and is placed in the integrated lava section (Fig 1D) using the data[19].

Olivine compositions

Magmas originated from mantle peridotite or reaction pyroxenite should crystallize magnesian olivine at low pressures[18,37]. The minimum forsterite component is expected for olivine in equilibrium with melt originated from the pure pyroxenitic source. Sobolev et al (2009) ref(*14*) estimated the composition of such an olivine to be in the range of Fo84-86 similar to the most magnesian composition of actual olivine from lavas of Gudchikhinkaya formation (up to Fo 83.5, ref(*14*)). This suggests minimal fractionation of these lavas. The subalkaline picrites from Ayan River on the Putorana plateau have also high-Mg olivine (up to Fo 90, see Fig S1) and thus a low degree of fractionation. The shallow-derived Siberian lavas (no garnet in the source) underwent more crystal fractionation and highly magnesian olivine is exceptionally rare in these lavas. Here we report olivine with up to Fo79 in upper, most voluminous volcanic formations of Norilsk area and corresponding lava suites at Maymecha-Kotuy and Putorana regions (see Fig S1). This value is more magnesian than previously reported in these suites. Figure S1 compares the compositions of the most magnesian olivines reported in this paper with compositions of olivine expected to crystallize from peridotite-derived magmas[18,37]. For the same Fo content, all Siberian olivines are significantly higher in Ni and lower in Mn (seen also in higher FeO/MnO ratio) than olivine from peridotite derived magmas. Crystallization of large amounts of early clinopyroxene could potentially create a similar affect in coexisting olivine. This is demonstrated by compositional trend of olivine from sample CY-315 from Tuklonskaya formation (Fig S1). This olivine has lowest Ni of the all Siberian samples and defines the flattest trend in Fo-NiO space. In this olivine CaO decreases rapidly and FeO/MnO increases with decreasing Fo. Thus for this lava we cannot exclude the possibility that the primary high-Mg melt was derived from a peridotite- dominated source. However, the CaO contents of olivine from other samples do not support this interpretation (see Fig S1C). Instead, we suggest that high Ni and low Mn in Siberian olivines imply a large fraction of non-peridotitic lithology in their source[18,37]. We note that FeO/MnO ratio of olivine does not change significantly during shallow fractional crystallization as indicated by the trends on Figure S1D. This supports the use of this ratio for estimating amount of pyroxenitic component for highly evolved low magnesian olivine. The most magnesian olivine reported here (Fo79) comes from the most voluminous traps lavas but it is still much less magnesian than expected for their primary melts. This may suggest that an early stage of their fractionation took place at deep magma chambers, perhaps at 40-50 km depth close to the level of their origin predicted by model.

Calculation of density

Apart from temperature, pressure and initial composition, the densities of all materials are assumed to be affected by variable content of melt, crystallized melt or melt extraction. All these effects are linearized and are considered in Boussinesq approximation. Density of material i is

$$\rho_i = \rho_i^0(P,T)(1-a_i^{pr}\cdot X_{pr}+a_i^{px}\cdot X_{px}+a_i^{epx}\cdot X_{epx}+a_i^{epr}\cdot X_{epr}+a_i^{mpx}\cdot X_{mpx}+a_i^{mpr}\cdot X_{mpr}) \qquad \text{(S1)}$$

Where $\rho_i^0(p,T)$ is density of pure non molten i-th material, X_{pr} is concentration of extracted peridotitic melt, X_{px} is concentration of the pyroxenitic component, X_{epx} is concentration of crystallized melt derived from the pyroxenitic component, X_{epr} is concentration of crystallized melt derived from the peridotitic component, X_{mpx} is concentration of melt derived from the pyroxenitic component, X_{mpr} is concentration of melt derived from the peridotitic component. All concentrations are volume concentrations. Multipliers of concentrations ("a" parameters) are constants depending on material and pressure. The "a" parameters related to melt were assumed to be -0.1 for all materials. Values for the "a" parameters related to crystallized melt and pyroxenitic component in mantle materials (mantle lithosphere, asthenosphere and plume) were estimated calculating rock densities for different pressure and temperature from bulk chemical compositions of pyroxenite-derived[14] and peridotite-derived basalts[70] using a thermodynamic modeling approach[71]. For density effect of melt extraction from peridotite (depletion) we use data[72]. All these parameters were found to be close to 0.05 (0.045-0.055) in the eclogite stability field. For simplicity, we assume them to be equal to 0.05 in the eclogite stability field (here at depth > 55 km). Change of density due to gabbro-eclogite transformation[71] is considered by linearly decreasing "a" parameters from 0.05 at depth of 55 km to -0.05 at depth of 40 km.

With the accepted values of parameters, the buoyancy of the thermo-chemical plume with an excess temperature of 250 °C (Tp=1600°C) and an eclogite content of 15 % is only 10% of the buoyancy of the purely thermal plume with the same temperature.

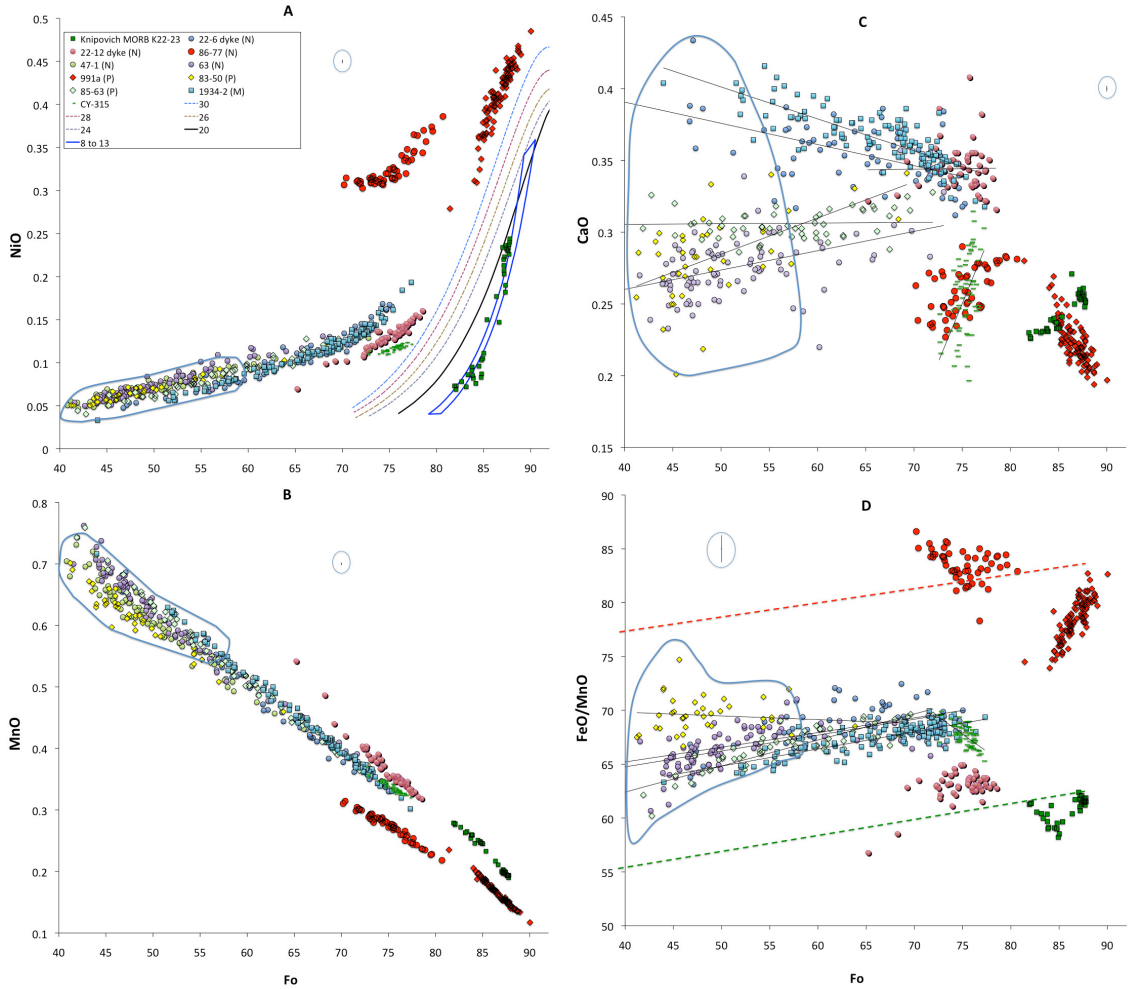

Fig.S1. Compositions of representative Siberian trap olivine, compared with olivine from peridotite derived melts. A. Numbered lines and field are compositions of olivine crystallized from peridotite derived melt with initial MgO content indicated by corresponding number[37]. Blue field outline compositions of low magnesian olivines (Fo<60) from Siberian traps (Supplementary Table S3). Knipovich MORB K22-23-stands for olivine compositions from Knipovich ridge MORB sample with almost zero content of pyroxenitic component in the melt[18]. C. Solid black lines indicate linear regression lines for the olivine of different samples. Other symbols are as on Fig S1A. D. Dashed red and green lines are suggested boundaries for FeO/MnO ratios of end-member olivines crystallized from pyroxenite and peridotite derived melts respectively. Slope of these lines constrained to be parallel to the dominant slope of trend lines. Other symbols are as on Fig S1A,B. Error bars outlined by the blue circle are 2-standard deviations estimated from repeated analyses of olivine standard.

Model setup

The setup and boundary conditions for our preferred model are presented in Fig. S2. We assume that the plume head arrives at the base of the cratonic root at model time 0. The left model boundary is open for inwards- and outwards flow of material, while the right boundary and bottom are closed, to avoid instabilities. We use a non-uniform grid to better resolve the central part of the model. Finite element size is 5 X 5 km in the best-resolved part of the model. Tests show no significant influence on model results of mesh coarsening out of that region. Plume potential temperature for the preferred model is Tp=1600°C and the content of recycled oceanic crust (eclogite) is 15 wt%. Evolution in time of temperature and pyroxenite content are shown in Fig. S3.

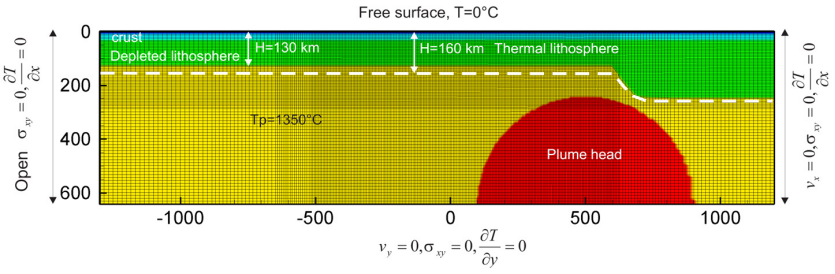

Fig. S2. Initial and boundary conditions for the preferred model. Background colors show initial distribution of rock-types. Dark blue-upper crust, blue- lower crust, green- depleted mantle lithosphere, yellow- asthenosphere, red- plume. White dashed line shows bottom of the thermal boundary layer, where potential temperature, reaches asthenospheric temperature of 1350 °C. Potential temperature in the plume head is 1600°C. Also shown is the finite element grid which is finest in the central-upper part of the model.

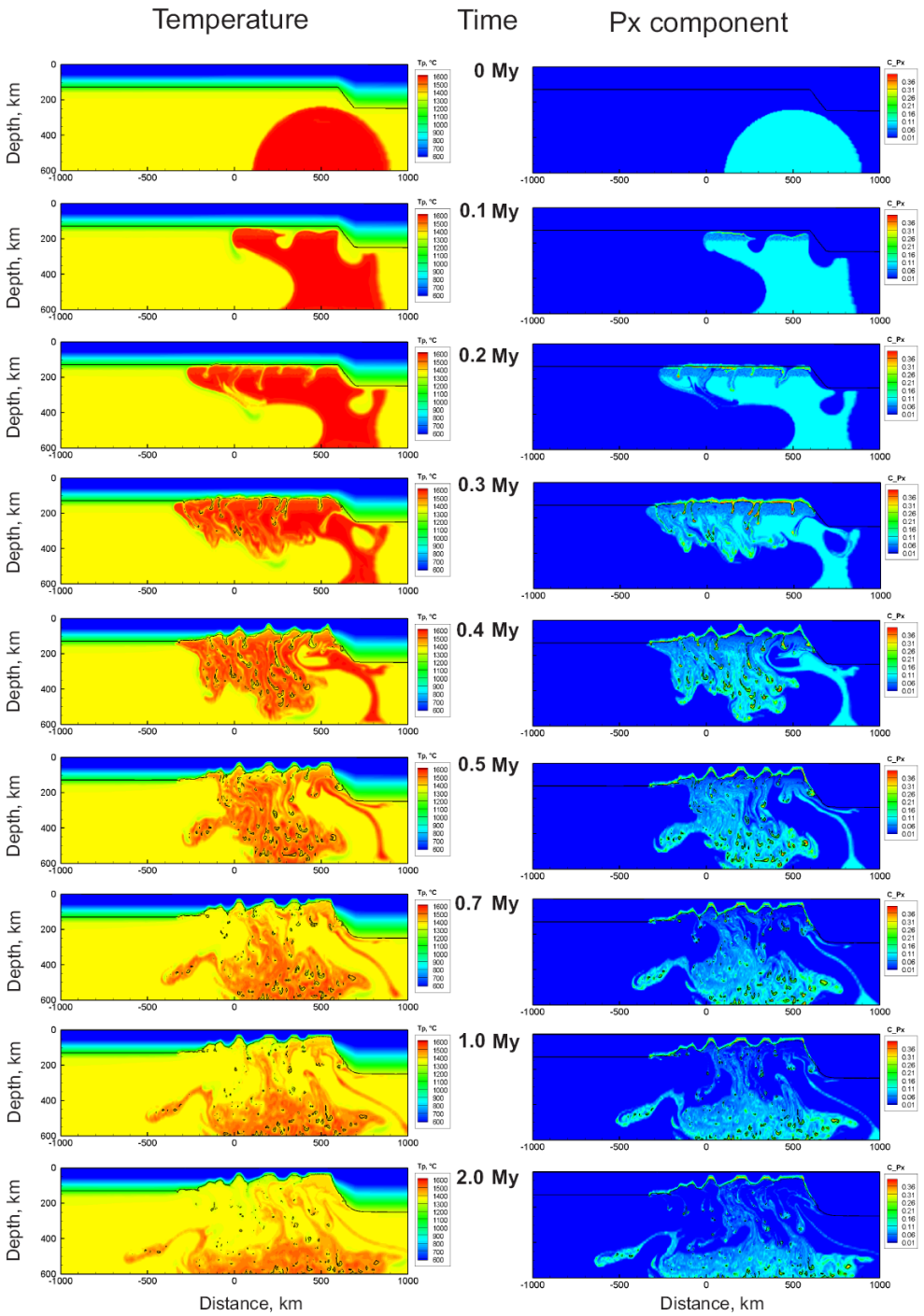

Fig. S3. Evolution of the potential temperature distribution *Tp* (left column) and of distribution of the pyroxenite component in the plume or in the crystallized melt C_Px (right column))

Model sensitivity and preferred model

The intensity of lithospheric destruction and melt production depend on (1) the initial thickness and degree of depletion of the lithosphere (Fig. S4), (2) plume temperature, and volume (Fig. S5), and (3) content of the recycled crust in the plume (Fig. S6).

Our preferred model is constrained by the petrological data, i.e. a plume head potential temperature of 1600°C, 15 wt% of recycled crust, and an initial thickness of depleted lithosphere of 130 km. A plume head radius of 400 km was chosen arbitrarily. With the fixed initial thickness of the lithosphere, a lower plume potential temperature (1500-1550°C instead of 1600°C in preferred model), or a smaller plume (200-300 km radius instead of 400 km) would result in much less extensive lithospheric delamination and lower melt production (Fig. S5). A content of recycled crust significantly higher than 15 wt% makes the plume negatively buoyant (at plume potential temperature of 1600°C), while a lower content results in large pre-magmatic uplift (Fig. S6).

We prefer a model of re-fertilized mantle lithosphere because the lithosphere of Siberian Craton experienced multiple interactions with mantle plumes before the emplacement of Siberian Traps, as evidenced by multiple phases of kimberlite magmatism and synchronous flood basalts[73,74]. Choosing depleted lithosphere with two-times larger density deficit does not significantly change the results (Fig. 3a main text, dashed curve and Fig. S4). However, further rise of the average degree of depletion and density deficit, to 60 and 70 kg/m^3, significantly impedes lithospheric destruction (Fig. S4).

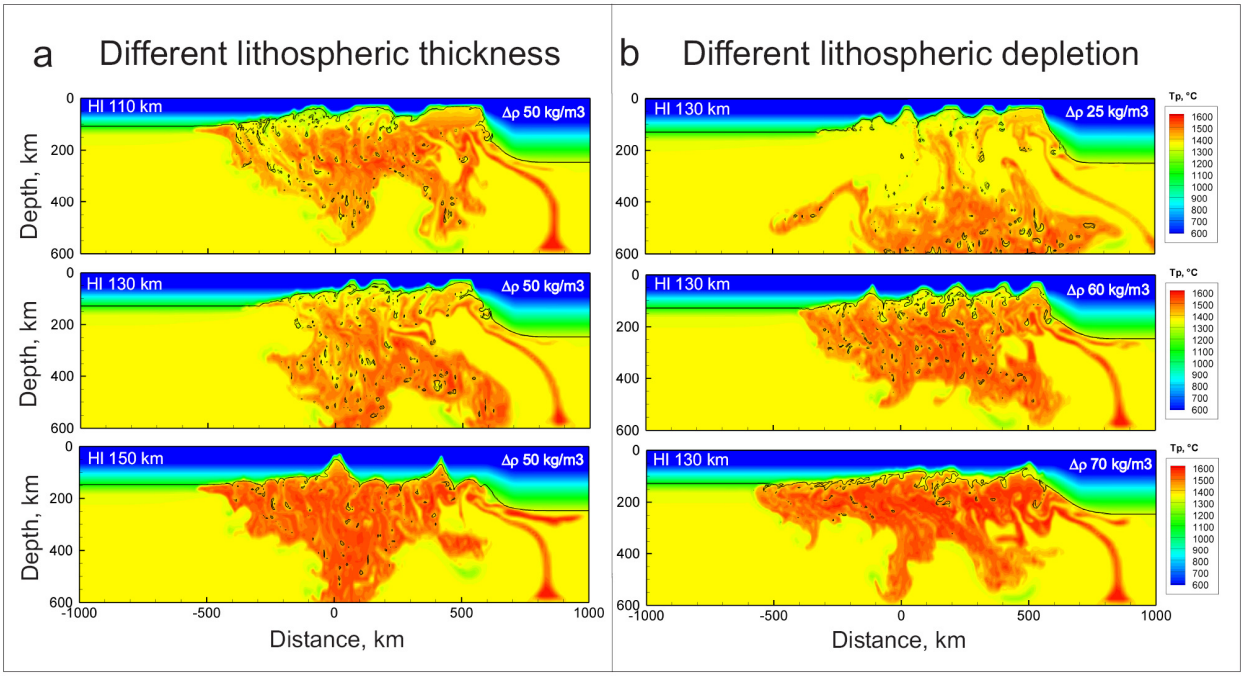

Fig. S4. Effect of thickness of the depleted lithosphere *Hl* (a) and degree of depletion (b) on the intensity of the lithospheric destruction. Shown are potential temperature distributions at model time 1.0 Myr.

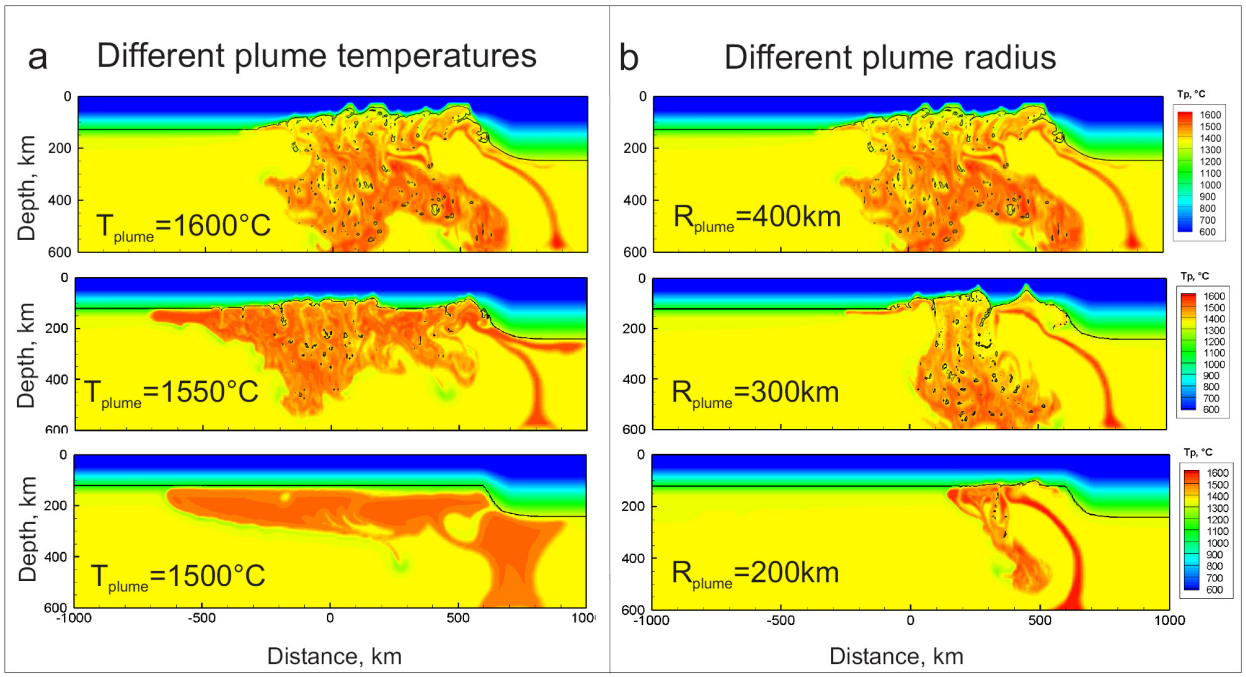

Fig. S5. Effect of a plume potential temperature, *Tp* (a) and a plume radius *R* (b) on the intensity of the lithospheric destruction. Shown are potential temperature distributions at model time 1.0 Myr.

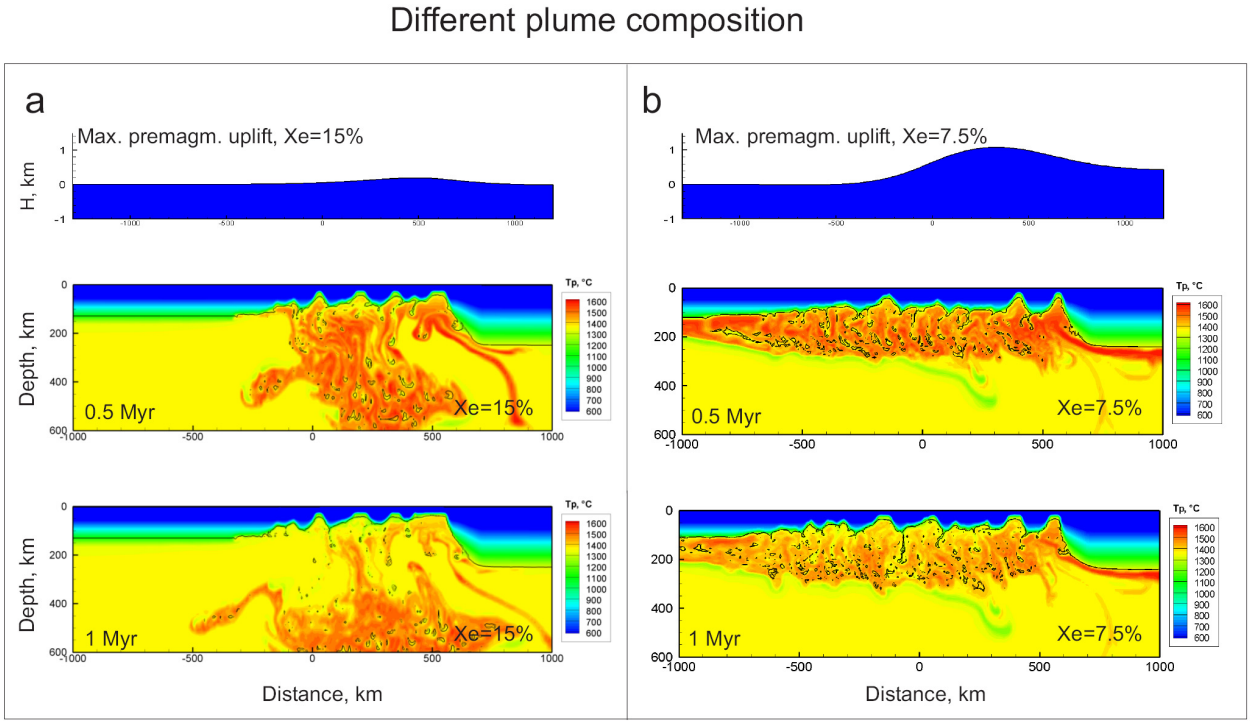

Fig. S6. Effect of a plume composition on pre-magmatic surface topography (*H*) and on intensity of the lithospheric destruction. Shown is the maximum pre-magmatic surface topography (upper panel) and temperature distributions at model times 0.5 and 1.0 Myr. Content of the recycled crust component in plume (*Xe*) is 15 Wt% (a) and 7.5 Wt% (b)**.**

58 Krivolutskaya, N. & Rudakova, A. Structure and Geochemical Characteristics of Trap Rocks from the Noril'sk Trough, Northwestern Siberian Craton. *Geochemistry International* **47**, 675-698, doi:10.1134/S0016702909070015 (2009).

59 Krivolutskaya, N. A., Sobolev, A. V., Mikhailiov, V. N. & Svirskaya, N. M. New data concerning the high-Mg rocks of the Siberian trap formation in the Noril'sk region. *Geochimica Et Cosmochimica Acta* **71**, A525-A525 (2007).

60 Hofmann, A. W. Chemical differentiation of the Earth: the relationship between mantle, continental crust, and oceanic crust. *Earth Planet. Sci. Lett.* **90**, 297-314 (1988).

61 Nesterenko, G. V., Tikhonenkov, P. I. & Kolesov, G. M. Rare-earth elements in plateau-basalt of the Siberian platform. *Geokhimiya*, 823-834 (1990).

62 Nesterenko, G. V., Tikhonenkov, P. I. & Romashova, T. V. Basalts of Putorana plateau. *Geokhimiya*, 1419-1425 (1991).

63 Sharma, M., Basu, A. R. & Nesterenko, G. V. Nd-Sr isotopes, petrochemistry, and origin of the Siberian flood basalts, USSR. *Geochimica Et Cosmochimica Acta* **55**, 1183-1192 (1991).

64 Sharma, M., Basu, A. R. & Nesterenko, G. V. Temporal Sr-isotopic, Nd-isotopic and Pb-isotopic variations in the Siberian flood basalts - implications for the plume-source characteristics. *Earth and Planetary Science Letters* **113**, 365-381 (1992).

65 Vasilev, Y. R. Plagioclase bearing picrites of Ayan river. *Russian Geology and Geophysics*, 68-75 (1988).

66 Vasiliev, Y. R. & Zolotukhin, V. V. The Maimecha-Kotui alkaline-ultramafic province of the northern Siberian Platform, Russia. *Episodes* **18**, 155-164 (1995).

67 Arndt, N., Chauvel, C., Czamanske, G. & Fedorenko, V. Two mantle sources, two plumbing systems: tholeiitic and alkaline magmatism of the Maymecha River basin, Siberian flood volcanic province. *Contributions to Mineralogy and Petrology* **133**, 297-313 (1998).

68 Vasilev, Y. R. Low potassium basalts of Maimecha-Kotuy province and their likely geodynamic setting. *Doklady Akademii Nauk* **366**, 507-510 (1999).

69 Hirth, G. & Kohlstedt, D. L. in *In Inside the Subduction Factory* Vol. 138 (ed J. Eiler) 83-105 (American Geophysical Union 2003).

70 Walter, M. J. Melting of garnet peridotite and the origin of komatiite and depleted lithosphere. *Journal of Petrology* **39**, 29-60 (1998).

71 Sobolev, S. V. & Babeyko, A. Y. Modeling of mineralogical composition, density and elastic-wave velocities in anhydrous magmatic rocks. *Surveys in Geophysics* **15**, 515-544 (1994).

72 Schutt, D. L. & Lesher, C. E. Effects of melt depletion on the density and seismic velocity of garnet and spinel lherzolite. *Journal of Geophysical Research-Solid Earth* **111**, B05401, doi: 10.1029/2003jb002950 (2006).

73 Griffin, W. L. *et al.* The Siberian lithosphere traverse: mantle terranes and the assembly of the Siberian Craton. *Tectonophysics* **310**, 1-35 (1999).

74 Kuzmin, M. I., Yarmolyuk, V. V. & Kravchinsky, V. A. Phanerozoic hot spot traces and paleogeographic reconstructions of the Siberian continent based on interaction with the African large low shear velocity province. *Earth-Science Reviews* **102**, 29-59, doi:10.1016/j.earscirev.2010.06.004 (2010).

Table S1. Studied samples and olivine.

Sample	Group	Region	Unit	Ref	Type	Thick m	N1	Max Fo	N2	Avg Fo (3)	Xpx Ni	S.e	Xpx Mn	S.e	Xpx	S.e	FeO/MnO	Gd/Yb n
SU-50	Deep	Nor	Gd	S3	lava	345	128	81.32	75	79.71	1.32	0.01	0.99	0.00	**1.15**	**0.17**	82.8	2.60
4270/13	Deep	Nor	Gd	S3	lava	375	47	80.47	33	79.18	1.34	0.01	0.98	0.00	**1.16**	**0.18**	82.7	2.34
86-77	Deep	Nor	Gd	new	lava	380	52	80.69	7	79.12	1.38	0.03	1.02	0.01	**1.20**	**0.18**	83.8	2.24
XS-51/130	Deep	Nor	Gd	S3	lava	408	120	83.32	85	81.51	1.16	0.00	0.89	0.00	**1.03**	**0.14**	79.6	2.27
991a	Deep	Put	Ay	new	lava	1540	98	90.04	44	87.85	0.71	0.01	0.90	0.01	**0.80**	**0.10**	79.9	4.25
991b	Deep	Put	Ay	new	lava	1560	103	89.45	42	87.26	0.73	0.01	0.88	0.01	**0.80**	**0.08**	79.3	4.41
81-133	Deep	Put	Ay	new	lava	1580	100	88.39	73	86.59	0.75	0.00	0.84	0.00	**0.80**	**0.05**	78.3	4.50
86-86	Sh (Fo>60)	Nor	Tk	new	lava	580	9	71.93	9	70.87	0.41	0.01	0.59	0.01	**0.50**	**0.09**	71.5	1.37
SU31	Sh (Fo>60)	Nor	Tk	S3	lava	586	75	76.66	14	74.92	0.32	0.01	0.49	0.01	**0.40**	**0.08**	68.9	1.28
SU33	Sh (Fo>60)	Nor	Tk	S3	lava	587	8	73.57	8	73.02	0.34	0.01	0.52	0.01	**0.43**	**0.09**	69.8	1.30
SU36	Sh (Fo>60)	Nor	Tk	new	lava	590	16	76.66	7	74.22	0.35	0.01	0.44	0.01	**0.40**	**0.04**	67.9	1.32
CY-315	Sh (Fo>60)	Nor	Tk	new	lava	592	62	77.28	54	75.59	0.27	0.00	0.42	0.01	**0.35**	**0.07**	67.4	1.36
530/12	Sh (Fo>60)	Nor	Nd	S3	lava	840	17	79.41	1	79.41	0.49		0.59		**0.54**	**0.05**	71.5	1.46
140-1	Sh (Fo>60)	Nor	Mr	new	lava	1200	34	67.96	2	67.74	0.61	0.04	0.55	0.08	**0.58**	**0.03**	70.4	1.33
4002-14	Sh (Fo>60)	Nor	Mk	new	lava	2049	36	62.78	1	62.78	0.64		0.48		**0.56**	**0.08**	68.8	1.30
47-1	Sh (Fo>60)	Nor	Mk	new	lava	2180	85	72.78	1	72.78	0.47		0.36		**0.41**	**0.06**	66.1	1.22
4002-18	Sh (Fo>60)	Nor	Hr	new	lava	2260	68	68.99	23	66.99	0.56	0.00	0.37	0.00	**0.46**	**0.10**	66.3	1.21
63	Sh (Fo>60)	Nor	Sm	new	lava	3030	89	73.09	2	72.38	0.54	0.02	0.37	0.02	**0.45**	**0.09**	66.2	1.19
85-63	Sh (Fo>60)	Put	Ay	new	lava	1500	57	71.94	3	70.29	0.56	0.03	0.51	0.00	**0.54**	**0.02**	69.5	1.14
83-50	Sh (Fo>60)	Put	Ho	new	lava	1800	39	69.26	2	68.83	0.57	0.03	0.44	0.01	**0.50**	**0.06**	67.9	1.32
1934-2	Sh (Fo>60)	M-K	On	new	lava	1600	115	77.33	5	75.61	0.57	0.03	0.45	0.02	**0.51**	**0.06**	68.1	1.20
141-7	Sh (Fo<60)	Nor	Nd	new	lava	1175	48	48.65	28	46.54	0.79	0.01	0.61	0.01	**0.61**		71.8	1.22
126-3	Sh (Fo<60)	Nor	Mr	new	lava	1232	67	52.82	6	50.77	0.80	0.02	0.58	0.03	**0.58**		71.1	1.28
126-4	Sh (Fo<60)	Nor	Mr	new	lava	1258	48	52.19	6	50.70	1.05	0.02	0.70	0.01	**0.70**		74.2	1.26
126-7	Sh (Fo<60)	Nor	Mr	new	lava	1321	36	50.44	12	49.06	0.91	0.01	0.56	0.01	**0.56**		70.6	1.21
4002-2	Sh (Fo<60)	Nor	Mk	new	lava	1659	59	56.25	1	56.25	0.62		0.44		**0.44**		67.9	1.20
4002-5	Sh (Fo<60)	Nor	Mk	new	lava	1736	69	57.59	5	56.88	0.67	0.02	0.44	0.03	**0.44**		67.9	1.23
4002-7	Sh (Fo<60)	Nor	Mk	new	lava	1818	52	59.60	3	58.74	0.78	0.02	0.55	0.01	**0.55**		70.4	1.28
4002-11	Sh (Fo<60)	Nor	Mk	new	lava	1906	73	54.00	11	52.17	0.93	0.02	0.55	0.01	**0.55**		70.5	1.25
46-1	Sh (Fo<60)	Nor	Mk	new	lava	2080	45	49.50	45	48.33	1.08	0.01	0.68	0.01	**0.68**		73.8	1.21
19-1	Sh (Fo<60)	Nor	Mk	new	lava	2130	12	48.75	7	46.70	1.01	0.04	0.61	0.02	**0.61**		72.0	1.22
136-13	Sh (Fo<60)	Nor	Mk	new	lava	2235	51	49.37	36	47.30	0.98	0.01	0.52	0.01	**0.52**		69.8	1.15
4002-19	Sh (Fo<60)	Nor	Hr	new	lava	2310	60	47.30	60	46.16	1.14	0.01	0.63	0.00	**0.63**		72.4	1.23
137-2	Sh (Fo<60)	Nor	Hr	new	lava	2430	27	51.33	9	50.02	1.08	0.02	0.56	0.01	**0.56**		70.6	1.06
61-3	Sh (Fo<60)	Nor	Hr	new	lava	2460	12	47.07	12	45.85	0.92	0.02	0.48	0.01	**0.48**		68.8	1.18
115-1	Sh (Fo<60)	Nor	Hr	new	lava	2650	111	59.01	1	59.01	0.71		0.34		**0.34**		65.7	1.16
115-9	Sh (Fo<60)	Nor	Hr	new	lava	2800	75	53.44	6	51.21	0.70	0.01	0.26	0.02	**0.26**		64.0	1.29
62	Sh (Fo<60)	Nor	Km	new	lava	2862	6	46.53	1	46.53	0.69		0.26		**0.26**		64.0	1.30
62-1	Sh (Fo<60)	Nor	Km	new	lava	2890	37	47.53	12	45.78	0.67	0.01	0.20	0.01	**0.20**		62.8	1.22
119-1	Sh (Fo<60)	Nor	Km	new	lava	2900	48	56.31	1	56.31	0.58		0.29		**0.29**		64.6	1.21
137-11	Sh (Fo<60)	Nor	Km	new	lava	2930	18	53.50	2	52.55	0.67	0.02	0.28	0.08	**0.28**		64.4	1.22
125-4	Sh (Fo<60)	Nor	Sm	new	lava	3140	74	58.55	12	57.24	0.79	0.01	0.37	0.01	**0.37**		66.3	1.19
65-4	Sh (Fo<60)	Nor	Sm	new	lava	3420	83	51.51	8	49.82	0.85	0.02	0.36	0.01	**0.36**		66.1	1.16
65-5	Sh (Fo<60)	Nor	Sm	new	lava	3480	48	55.36	1	55.36	0.68		0.47		**0.47**		68.5	1.18
81-134	Sh (Fo<60)	Put	Ay	new	lava	1300	26	59.80	1	59.80	0.69		0.51		**0.51**		69.6	1.15
22-6	Sh (Fo<60)	Nor	Hr-Sm	new	dyke	-	71	75.27	15	73.67	0.58	0.01	0.49	0.01	**0.53**	**0.05**	68.9	1.19
22-12	Sh (Fo<60)	Nor	Hr-Sm	new	dyke	-	51	78.52	28	76.64	0.37	0.00	0.21	0.01	**0.29**	**0.08**	63.2	1.13
12-1	Sh (Fo<60)	Nor	Hr-Sm	new	dyke	-	56	48.62	12	46.72	0.69	0.02	0.35	0.01	**0.35**		66.0	1.26
39-3	Sh (Fo<60)	Nor	Hr-Sm	new	dyke	-	98	54.21	87	52.46	0.84	0.00	0.36	0.00	**0.36**		66.2	1.22
125-5	Sh (Fo<60)	Nor	Hr-Sm	new	dyke	-	50	48.12	24	45.80	0.78	0.01	0.51	0.01	**0.51**		69.6	1.18
120	Sh (Fo<60)	Nor	Hr-Sm	new	dyke	-	75	61.16	34	59.49	0.73	0.00	0.28	0.00	**0.28**		64.5	1.16

Table S1 notes. Group: deep (high Gd/Ybn>1.6 =garnet signature), Sh- shallow (low Gd/Ybn< 1.6 = no garnet in the source), Fo- maximum amount of Forsterite content in olivine in the sample. Region: Nor-Norilsk, Put-Putorana plateau, M-K- Maymecha-Kotuy province. Unit: (Norilsk region Gd-Gudchikhinskaya, Tk-Tuklonskaya, Nd-Nadezhdinskaya, Mr-Morangovskaya, Mk-Mukulaevskaya, Hr-Haerlakhskaya, Km-Kumginskaya, Sm-Samoedskaya; Putorana plateau Ay-Ayanskaya, Ho-Honumanskaya; Maymecha-Kotuy province On- Onkuchakskaya. Ref: references. Type: lavas or dykes. Thick: thickness in meters. N1: Total amount of olivine grains analyzed. Max Fo : composition of most magnesian olivine. N2: amount of olivine grains having composition within maximum 3 mol% Fo. Avg Fo (3)- average of most magnesian olivine grains having composition within maximum 3 mol% Fo. Xpx Ni and Xpx Mn- proportion of pyroxenite derived melt calculated from Ni excess and Mn deficiency correspondingly in average most magnesian olivine. Xpx-accepted proportion of pyroxenite derived melt (see text). S.e.- standard error of mean. FeO/MnO- corresponding ration for the average most magnesian olivine. Gd/Ybn- normalized to primitive mantle [5] ratio of bulk rock.

Table S2. Model parameters.

Parameter	Upper crust	Lower crust	Depleted mantle lithosphere	Asthenosphere / plume
Density, [kg/m^3]	2750	2950	3330-$\Delta\rho_{depl}$	3330
Thermal expansion, [K^{-1}]	$3.7\cdot10^{-5}$	$2.7\cdot10^{-5}$	$3.3\cdot10^{-5}$	$3.3\cdot10^{-5}$
Elastic moduli, K, G, [GPa]	55, 36	63, 40	122, 74	122, 74
Heat capacity, [J/kg/K]	1200	1200	1200	1200
Heat conductivity, [W/K/m]	2.5	2.5	3.3	3.3
Heat productivity, [W/m^3]	1.3	0.2	0	0
Initial friction angle, [degree]	30	30	30	30
Initial cohesion, [MPa]	20	20	20	20
Diffusion creep, log(A), [Pa^{-n}s^{-1}]	-	-	-10.59	-10.59
Diffusion creep activation energy, [kJ/mol]	-	-	300	300
Grain size[mm];Grain size exponent	-	-	1.0;2.5	1.0;2.5
Dislocation creep, log(A), [Pa^{-n}s^{-1}]	-28.0	-15.4	-15.2	-14.7/-14.3
Dislocation creep activation energy, [kJ/mol]	223	356	530	515
Power law exponent	4.0	3.0	3.5	3.5

Table S2 notes. Sources for dislocation creep laws: upper crust –quartzite[21]; lower crust– wet plagioclase[22]; depleted mantle lithosphere – dry peridotite[23], asthenosphere – wet peridotite with 1000 Ppm H_2O (asthenosphere) and 2000 Ppm H_2O (plume)[23].

Table S3. Compositions of olivine and host lavas. (Excel file).